ISSN 0021-3640, JETP Letters, 2019, Vol. 110, No. 2, pp. 140–153. © Pleiades Publishing, Inc., 2019.
Russian Text © The Author(s), 2019, published in Pis'ma v Zhurnal Eksperimental'noi i Teoreticheskoi Fiziki, 2019, Vol. 110, No. 2, pp. 126–139.

CONDENSED MATTER

# Occurrence of Topologically Nontrivial Phases, Cascade of Quantum Transitions, and Identification of Majorana Modes in Chiral Superconductors and Nanowires (Scientific Summary)

**V. V. Val'kov[a], *, V. A. Mitskan[a], A. O. Zlotnikov[a], M. S. Shustin[a], and S. V. Aksenov[a]**

[a] *Kirensky Institute of Physics, Federal Research Center KSC, Siberian Branch, Russian Academy of Sciences, Akademgorodok, Krasnoyarsk, 660036 Russia*

**e-mail: vvv@iph.krasn.ru*

Received June 11, 2019; revised June 11, 2019; accepted June 11, 2019

The problems of occurrence and experimental identification of topologically nontrivial phases in condensed matter have been reviewed. The results of the study of the effect of strong intra- and interatomic Coulomb interaction on a quantum phase transition with change in the topological index in an ensemble of Hubbard fermions on a triangular lattice have been reported. Nontrivial topology of the phase of coexistence of $d + id$ chiral superconductivity and 120° spin ordering in a system with the triangular lattice has been discussed and the formation of Majorana modes in such a phase has been demonstrated. A cascade of quantum transitions that occurs at the variation of the magnetic field or the electrochemical potential has been analyzed for an open nanowire with the Rashba spin–orbit coupling and the induced superconducting pairing potential. It has been shown that anomalies of magneto- and electrocaloric effects are manifested near such quantum transitions and can be used to experimentally test materials on the existence of topologically nontrivial phases in them. The switching of the spin-polarized current in the topological superconducting phase has been predicted for a semimetal/superconducting wire/semimetal structure in the weak nonequilibrium regime.

**DOI:** 10.1134/S002136401914011X

## 1. INTRODUCTION

After the first theoretical studies of topological insulators [1–3] and topological superconductors [4–7], whose existence was predicted for relatively simple systems described by quadratic forms of the secondary quantization operators, new directions of study of topologically nontrivial phases in condensed matter appeared. There were several reasons for the expansion of the field of studies.

First, it was necessary to consider models where real features of materials are taken into account more completely. In particular, the study of topological phases with the inclusion of the Coulomb interaction between fermions seemed relevant. It often appeared that materials considered as candidates for the occurrence of topological phases because of a significant intra-atomic repulsion between electrons were materials with strong electron correlations [8–14].

The second reason was the desirability of materials where topological phases would occur under more experimentally achievable conditions. To this end, new mechanisms inducing nontrivial topology in superconductors were sought. The simultaneous effect of an external magnetic field, spin–orbit coupling, and proximity-induced superconducting pairing potential played a significant role in the first studies of topological superconductors with the *s*-wave symmetry of the order parameter in nanowires [6, 7]. Alternatively, solid-state systems where superconducting pairing is due to internal interactions in a material were recently studied [15–24].

A significant amount of attention was paid to materials where the superconducting phase coexists with noncollinear spin ordering [17, 18]. In this case, the formation of the superconducting phase with a nontrivial topology does not require the presence of the spin–orbit coupling and external magnetic field. This was possible because the strong spin–fermion correlation ensured the mixing of states with different spin projections.

The investigation of the conditions for occurrence of topologically nontrivial phases in materials with strong electron correlations required not only expanding mathematical methods but also generalizing the definition of topological indices because approaches previously developed for Hamiltonians representable as quadratic forms of secondary quantization operators became inapplicable [25, 26].

The study of topological systems is directly associated with search for experimental proof of the occurrence of a nontrivial phase. In particular, the practical detection of attributes indicating the existence of the Majorana mode in the system prepared from a topological superconductor in the open boundary geometry is of current interest. In this respect, the tunneling spectroscopy method is promising. The features of the current–voltage characteristic revealed by this method [27] were treated as manifestations of the Majorana mode. The topological system was a semiconductor wire with the strong spin–orbit coupling in an external magnetic field and with the proximity-induced superconducting pairing potential [7, 28]. The results obtained in [27] stimulated active studies of the identification of the Majorana mode because the interpretation of the tunnel spectroscopy data seemed ambiguous [29]. For this reason, search for alternative methods for identification of topological phases seems relevant.

In this work, we review recent studies of the aforementioned problems of occurrence of topologically nontrivial phases in condensed matter. The effect of the strong intra- and interatomic Coulomb interactions on the topological characteristics of superconductors with the chiral symmetry of the order parameter and on topological transitions between different phases is considered in Section 2. The studies of the possibility of occurrence of nontrivial topology and the Majorana mode in the phase of coexistence of chiral superconductivity and noncollinear spin ordering in layered materials with the triangular lattice are reviewed in Section 3. The studies of the structure of the ground state of the quantum wire with the spin–orbit coupling in the topological phase are discussed in Section 4, where the features of the magnetocaloric effect in this nanowire are also described. The features of the spin-polarized transport that are caused by the existence of the Majorana mode in the nanowire are presented in Section 5.

## 2. QUANTUM TOPOLOGICAL TRANSITION IN THE SUPERCONDUCTING CHIRAL $d + id$ PHASE

Water-intercalated sodium cobaltite $Na_xCoO_2 \cdot yH_2O$ is one of the materials where the Coulomb interaction between electrons qualitatively affects the topological transition in the superconducting phase [30, 31]. In the absence of doping, the $3d^5$ electron configuration of $Co^{4+}$ ions in the octahedral environment with trigonal distortion corresponds to the filling of the lower orbital doublet with four electrons and the filling of the split orbital singlet with one electron. This level is degenerate in spin projection, and Hubbard splitting into two subbands occurs in the crystal with the strong intra-atomic Coulomb repulsion. The lower subband is filled. Therefore, the ground state of the $CoO_2$ layer corresponds to an antiferromagnetic Mott insulator.

Doping is accompanied by the filling of the upper Hubbard subband. The long-range magnetic order in a two-dimensional system is destroyed at finite temperatures and it can be disregarded in the superconducting phase.

The considered electron doping regime with the filling of the upper Hubbard subband is often described by the $t$–$J$ model. In reality, when deriving the effective model, three-center terms appear and are significant for the description of the superconducting phase [32]. For this reason, we use below the $t$–$J^*$–$V$ model involving not only three-center terms $\mathcal{H}_3$ but also the intersite Coulomb repulsion. In the representation of the Hubbard operators [33, 34], the Hamiltonian has the form

$$\mathcal{H} = \mathcal{H}_0 + \mathcal{H}_T + \mathcal{H}_J + \mathcal{H}_{(3)} + \mathcal{H}_V, \tag{1}$$

where

$$\mathcal{H}_0 = \sum_{f\sigma}(\epsilon - \mu) X_f^{\sigma\sigma} + \sum_f (2\epsilon + U - 2\mu) X_f^{22},$$
$$\mathcal{H}_T = \sum_{fm\sigma} t_{fm} X_f^{2\bar{\sigma}} X_m^{\bar{\sigma}2}, \tag{2}$$

$$\mathcal{H}_J = \frac{1}{2}\sum_{fm\sigma} J_{fm}\left(X_f^{\bar{\sigma}\sigma} X_m^{\sigma\bar{\sigma}} - X_f^{\bar{\sigma}\bar{\sigma}} X_m^{\sigma\sigma}\right),$$

$$\mathcal{H}_{(3)} = \sum_{\substack{fmg\sigma \\ (f\neq g)}} \frac{t_{fm}t_{mg}}{U}\left(X_f^{2\bar{\sigma}} X_m^{\sigma\sigma} X_g^{\bar{\sigma}2} - X_f^{2\bar{\sigma}} X_m^{\bar{\sigma}\sigma} X_g^{\sigma 2}\right), \tag{3}$$

$$\mathcal{H}_V = \frac{1}{2}\sum_{f\delta} V\left(\hat{n}_f - \langle \hat{n}_f \rangle\right)\left(\hat{n}_{f+\delta} - \langle \hat{n}_{f+\delta} \rangle\right). \tag{4}$$

Here, $\mathcal{H}_0$ is the energy operator of electrons at the sites of the triangular lattice; $\mathcal{H}_T$ and $\mathcal{H}_J$ are the kinetic and exchange terms, respectively; $\mathcal{H}_{(3)}$ describes correlated hoppings; $\mathcal{H}_V$ describes the Coulomb repulsion between electrons in neighboring sites; the usual notation is used for the Hubbard operators for the upper Hubbard subband; $\epsilon$ is the energy of the single-electron state; $\mu$ is the chemical potential of the ensemble; $U$ and $V$ are the parameters of the intra- and interatomic Coulomb interactions between electrons, respectively; and $\hat{n}_f = X_f^{\uparrow\uparrow} + X_f^{\downarrow\downarrow} + 2X_f^{22}$ is the electron number operator at the $f$th site.

When the exchange coupling within two coordination spheres is taken into account, the solution of the equation for the superconducting order parameter with the $d_{x^2-y^2} + id_{xy}$ symmetry is written in the form

$$\Delta_d(q) = 2\Delta_{d1}^0 \varphi_{d1}(q) + 2\Delta_{d2}^0 \varphi_{d2}(q), \tag{5}$$

where the basis functions

$$\varphi_{d1}(q) = \cos q_y - \cos\left(\sqrt{3}q_x/2\right)\cos\left(q_y/2\right) + i\sqrt{3}\sin\left(\sqrt{3}q_x/2\right)\sin\left(q_y/2\right), \quad (6)$$

$$\varphi_{d2}(q) = \cos\sqrt{3}q_x - \cos\left(\sqrt{3}q_x/2\right)\cos\left(3q_y/2\right) - i\sqrt{3}\sin\left(\sqrt{3}q_x/2\right)\sin\left(3q_y/2\right)$$

correspond to the first and second coordination spheres [35]. Since these functions are complex, they vanish not on lines but only at certain points of the Brillouin zone. In this case, the position of nodal point $\Delta_d(q)$ depends on the ratio of the amplitudes $\Delta^0_{d1}$ and $\Delta^0_{d2}$ (see Fig. 1). When only the basis function of the first coordination sphere $\varphi_{d1}$ contributes to $\Delta_d(q)$, nodal points are located in the center and edges of the Brillouin zone and are not crossed by the Fermi contour at any finite concentrations. If $\Delta^0_{d1} = 0$ and $\Delta^0_{d2} \neq 0$, nodal points exist inside the Brillouin zone. In the general case, the ratio $\Delta^0_{d1}/\Delta^0_{d2}$ depends on the charge carrier density and the model parameters. Under the variation of the density, the mutual dynamics of the Fermi contour and nodal points appears; as a result, a quantum topological transition occurs in the system when the Fermi contour crosses nodal points.

An important role of the intersite Coulomb repulsion between fermions in the occurrence of the quantum topological transition is manifested through the mechanism of the formation of nodal points $\Delta_d(q)$. The main effect of this interaction tends to eliminate the superconducting phase (here we do not discuss higher orders of perturbation theory that are responsible for the Kohn–Luttinger mechanism [36–38]). The interaction between electrons located on the nearest sites more strongly affects the superconducting pairing amplitude $\Delta^0_{d1}$, whereas the Coulomb repulsion for the second coordination sphere is more strongly manifested in a decrease in $\Delta^0_{d2}$. As a result, the ratio $\Delta^0_{d1}/\Delta^0_{d2}$ changes and nodal points $\Delta_d(q)$ are shifted. This is the mechanism of the influence of the intersite Coulomb interaction on the topological transition point under the variation of the carrier density in the system.

According to the spectrum of excitations in the superconducting phase $E_q = \sqrt{\xi_q^2 + |\Delta(q)|^2}$ ($\xi_q = \varepsilon_q - \mu$, $\varepsilon_q$ is the energy of the electron in the normal phase), the spectrum of the superconducting phase becomes gapless when the Fermi contour of the normal phase crosses nodal points of $\Delta(q)$.

The complex character of $\Delta_d(q)$ initiates topological peculiarities of the superconducting phase. The

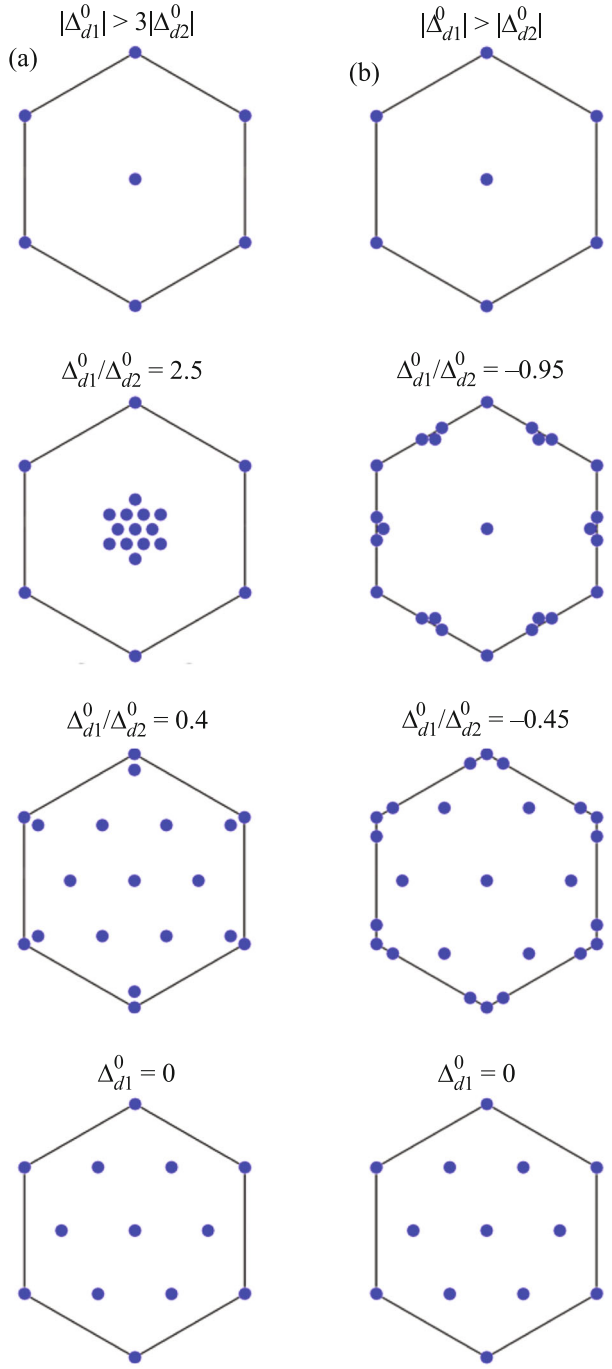


**Fig. 1.** (Color online) Configurations of nodal points $\Delta_d(q)$ at different ratios of $\Delta^0_{d1}$ and $\Delta^0_{d2}$ having the (a) same and (b) opposite signs.

introduction of the unit vector $\mathbf{m} = (m_x, m_y, m_z)$ [39] with the components

$$m_x = \frac{\mathrm{Re}\Delta_d(q)}{E_q}, \quad m_y = \frac{-\mathrm{Im}\Delta_d(q)}{E_q}, \quad m_z = \frac{\xi_q}{E_q} \quad (7)$$

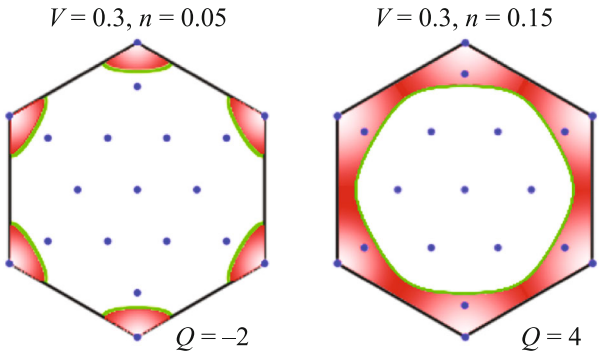


**Fig. 2.** (Color online) topological indices $Q$ for two configurations of nodal points $\Delta_d(q)$ and Fermi contour. The parameters are $J_1 = 0.3|t_1|$, $J_2 = 0.2|t_1|$, and $t_2 = t_3 = 0$.

makes it possible to construct a mapping between the points of the Brillouin zone and the points of a two-dimensional sphere with the unit radius. Thus, motion on the Brillouin zone is mapped to motion on this sphere. Different homotopic classes of such trajectories are classified in terms of the degree of mapping called the topological index [35]

$$Q = \frac{1}{8\pi}\sum_{\Delta}\mathbf{m}_1 \cdot [\mathbf{m}_2 \times \mathbf{m}_3], \qquad (8)$$

where summation is performed over all triangular plaquettes and the vectors $\mathbf{m}_1$, $\mathbf{m}_2$, and $\mathbf{m}_3$ are calculated at the vortices of plaquettes. The index $Q$ reflects the topological structure of the superconducting phase and is related to the mutual arrangement of nodal points $\Delta_d(q)$ and the Fermi contour. If the variation of the density results in the crossing of nodal points by the Fermi contour of the normal phase (Fig. 2), a quantum topological transition occurs [40, 41].

As known [42], the nonzero values of the topological invariant $Q$ in the chiral superconducting phase of the system with periodic boundary conditions indicate the presence of edge states in a similar system with open boundaries. In the next section, we describe the mechanism of the formation of edge states and Majorana modes in the spin-singlet superconducting phase with the $d + id$ symmetry.

## 3. MAJORANA MODES IN THE PHASE OF COEXISTENCE OF CHIRAL SUPERCONDUCTIVITY AND SPIN ORDERING ON THE TRIANGULAR LATTICE

Soon after the formation of Majorana modes in superconducting systems with the spin–orbit coupling in a uniform magnetic field was predicted [6, 7], it was demonstrated that a nonuniform external field can play a role similar to the spin–orbit coupling [43]. Correspondingly, alternative systems for the occurrence of Majorana modes were proposed: (i) a chain of magnetic nanoparticles with arbitrary directions of the magnetization on a superconducting substrate [44], (ii) nanowires with the induced superconductivity in the spatially nonuniform magnetic field [45], and (iii) quasi-one-dimensional systems with the Ruderman–Kittel–Kasuya–Yosida exchange interaction and helical magnetic order in contact with a superconductor [46, 47].

Materials with the phase of coexistence of superconductivity and noncollinear spin ordering such as $HoMo_6S_8$ and $ErRh_4B_4$ constitute another class of systems, where Majorana modes are induced through a similar scenario [17].

It was shown in [18] that, if the stripe magnetic order appears in the $Na_xCoO_2 \cdot yH_2O$ compound with the triangular lattice in the presence of the $d + id$ chiral superconductivity, Majorana modes are also formed. However, further analysis [48] showed that chiral superconductivity cannot coexist with stripe spin ordering but coexists with the magnetic order corresponding to the 120° structure. Furthermore, the calculations within the Hubbard and $t$–$J$ models demonstrate the occurrence of 120° spin ordering for the triangular lattice at low doping levels [49, 50]. The formation of the phase of coexistence of chiral superconductivity and 120° structure in this doping range was demonstrated in [51, 52].

The advantage of this mechanism in search for Majorana fermions is the unnecessity of the creation of complex structures with the proximity effect because superconductivity and magnetic ordering homogeneously coexist throughout the entire volume of the sample owing to internal interactions.

For clear illustration, we demonstrate the appearance of a nontrivial topology and Majorana modes in the phase of coexistence of $d + id$ chiral superconductivity and 120° magnetic ordering on the triangular lattice within the simple model [53]

$$\mathcal{H}_{\text{SC–NCO}} = -\mu\sum_{l\sigma} a^\dagger_{l\sigma}a_{l\sigma} + \sum_{lm\sigma} t_{lm}a^\dagger_{l\sigma}a_{m\sigma}$$
$$- h(\mathbf{Q})\sum_l \left(\exp(i\mathbf{QR}_l)a^\dagger_{l\uparrow}a_{l\downarrow} + \exp(-i\mathbf{QR}_l)a^\dagger_{l\downarrow}a_{l\uparrow}\right) \qquad (9)$$
$$+ \sum_{lm}\left(\Delta_{lm}a_{l\uparrow}a_{m\downarrow} + \Delta^*_{lm}a^\dagger_{m\downarrow}a^\dagger_{l\uparrow}\right),$$

where $a_{l\sigma}$ is the annihilation operator for an electron on the $l$th site (Wannier representation) and the spin projection $\sigma$, $\mu$ is the chemical potential, $t_{fm}$ and $\Delta_{fm}$ are the amplitudes of electron hoppings and superconducting pairings, $h(\mathbf{Q})$ is the exchange field parameter, and $\mathbf{Q}$ is the magnetic structure vector.

Hamiltonian (9) has the electron–hole symmetry and corresponds to the D class [54]:

$$\Lambda H(\mathbf{k})\Lambda = -H^*(-\mathbf{k} + \mathbf{Q}); \quad \Lambda = \begin{pmatrix} O & I \\ I & O \end{pmatrix}, \qquad (10)$$

where $H(\mathbf{k})$ is the Bogoliubov–de Gennes Hamiltonian matrix in the quasimomentum representation, and $O$ and $I$ are the zero and identity matrices, respectively.

A direct consequence of symmetry (10) is that the value $-\varepsilon_n(-\mathbf{k}+\mathbf{Q})$ is associated with each excitation energy $\varepsilon_n(\mathbf{k})$. We refer to points of the Brillouin zone that satisfy the relation $\mathbf{k} = -\mathbf{k} + \mathbf{Q} + \mathbf{G}$, where $\mathbf{G}$ is the reciprocal lattice vector, as particle–hole invariant momentum (PHIM) points and denote them as $\mathbf{K} = (K_1, K_2)$. In the toroidal topology with periodic boundary conditions along both directions of the lattice, there are four PHIM points $\mathbf{K}_I = (-2\pi/3, -2\pi/3)$, $\mathbf{K}_{II} = (-2\pi/3, \pi/3)$, $\mathbf{K}_{III} = (\pi/3, -2\pi/3)$, and $\mathbf{K}_{IV} = (\pi/3, \pi/3)$.

The formation of a topologically nontrivial phase for which the formation of Majorana modes is expected can be indicated by a negative fermion parity of the ground state (this was proposed for the first time in [4]). Since states with the quasimomenta $\mathbf{k}$ and $-\mathbf{k}+\mathbf{Q}$ are filled together and do not change the parity of the ground state, it is sufficient to analyze the filling of states at PHIM points. The superconducting order parameter vanishes at the PHIM point $\mathbf{K}_I$ and one state with the energy $\varepsilon_n(\mathbf{K}_I) < 0$ is filled under the condition $h > |\mu + 3t_1 - 6t_2 + 3t_3|$. States at the other PHIM points are not filled under this condition. At three points $\mathbf{K}_{II-IV}$, the Hamiltonian is reduced to the Hamiltonian of the superconductor in the uniform magnetic field and states are filled together under the condition $h > \sqrt{(\mu + t_1)^2 + 4\left(\Delta_{d1}^{(0)} - 2\Delta_{d2}^{(0)}\right)^2}$. The presented conditions specify regions where the ground state is represented as the superposition of states with an odd number of fermions and a topologically nontrivial phase occurs.

As known [5], the topological invariant $\mathbb{Z}_2$ (the Majorana number $\mathcal{M}$) is defined in terms of the fermion parity $P(\mathbf{K})$ of the ground state of the lattice in the toroidal topology:

$$\mathcal{M} = \prod_{\mathbf{K}} P(\mathbf{K}), \tag{11}$$

where $P(\mathbf{K})$ is calculated as the sign of the Pfaffian of the Bogoliubov–de Gennes matrix in the representation of Majorana operators. The value $\mathcal{M} = -1$ corresponds to the topologically nontrivial phase. At $\mathcal{M} = 1$, the state of the system is topologically trivial and Majorana modes do not occur. The direct calculation of $\mathcal{M}$ is in agreement with the above conditions for the occurrence of the topologically nontrivial phase obtained from the comparatively simple analysis of the parity of the ground state.

In the quasi-one-dimensional system with periodic boundary conditions along one of the directions of the lattice (cylindrical topology), Majorana modes occur only at $K_2 = -2\pi/3$ and in the same parametric regions as above. The topological invariant in this case has the form

$$\mathcal{M}(K_2) = P(K_2, K_1 = -2\pi/3)\, P(K_2, K_1 = \pi/3). \tag{12}$$

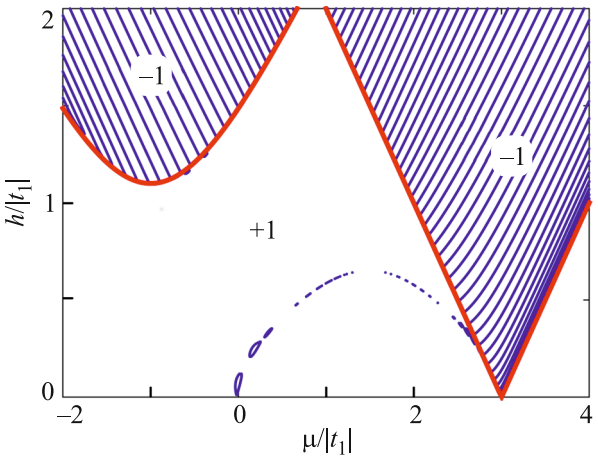


**Fig. 3.** (Color online) Diagram of states of the triangular lattice in the coexistence phase with different Majorana numbers. The thick lines are the boundaries of topologically nontrivial phases. Thin lines correspond to the parameters of the system for which excitations with zero energy occur in the cylindrical topology.

Thick lines in Fig. 3 are the boundaries of phases with different Majorana numbers on the "magnetic field–chemical potential" plane. The calculations were performed with the following amplitudes of superconducting pairings: $\Delta_{d1}^{(0)} = 0.05|t_1|$, $\Delta_{d2}^{(0)} = 0.3|t_1|$ at $t_2 = t_3 = 0$. Thin lines in Fig. 3 correspond to the parametric conditions of occurrence of zeroth modes for the lattice in cylindrical topology at $K_2 = -2\pi/3$ with the number of sites $N_1 = 48$ along the direction $\mathbf{a}_1$. It is seen that most of zeroth modes lie in the region of the parameters that corresponds to the topologically nontrivial phase of the system in closed geometry. With increasing $N_1$, all zeroth modes are distributed over regions with $\mathcal{M} = -1$. Such zeroth modes also occur in other models of quasi-one-dimensional systems with $D$ symmetry. In the next sections, we will show how these modes can be detected by measuring caloric effects and transport properties.

Topologically protected edge states can also occur at $\mathcal{M} = 1$. Their formation is indicated by nonzero values of the $\mathbb{Z}$ invariant for two-dimensional systems (in particular, including the interaction), which can be expressed in terms of the Green's functions [25, 55]:

$$\tilde{N}_3 = \frac{1}{24\pi^2}\varepsilon_{\mu\nu\lambda}\int_{-\infty}^{\infty} d\omega \int_{-\pi}^{\pi}\int_{-\pi}^{\pi} dk_1 dk_2 \mathrm{Sp}(G\partial_\mu G^{-1} \times G\partial_\nu G^{-1} G\partial_\lambda G^{-1}), \tag{13}$$

where $\mu, \nu, \lambda = 1, 2, 3$; $\varepsilon_{\mu\nu\lambda}$ is the antisymmetric Levi-Civita tensor; $\partial_1 = \partial/\partial_\omega$; $\partial_2 = \partial/\partial_{k_1}$; $\partial_3 = \partial/\partial_{k_2}$; and summation over repeated subscripts is implied. In the considered system of noninteracting electrons, $G = [i\omega I - H(\mathbf{k})]^{-1}$.

It is noteworthy that Eq. (13) for the Green's functions of a chiral superconductor without long-range magnetic order is reduced to the well-known definition for the winding number of the vector $\mathbf{m}$, which is introduced in Eq. (7) and is related to the Berry phase and Chern number:

$$Q = \frac{1}{4\pi}\int_{-\pi}^{\pi}\int_{-\pi}^{\pi} dk_1 dk_2 \mathbf{m}\cdot\frac{\partial \mathbf{m}}{\partial k_1}\times\frac{\partial \mathbf{m}}{\partial k_2}. \quad (14)$$

This expression is equivalent to the topological index introduced in Eq. (8).

A relation between the $\mathbb{Z}_2$ invariant (11) and topological index in the two-dimensional case (13) was established in [56] for noncentrosymmetric superconductors with $d$ symmetry. This relation for the considered system with the magnetic order has a similar form

$$(-1)^{\tilde{N}_3} = \mathcal{M}. \quad (15)$$

Consequently, Majorana modes are formed in topologically nontrivial phases with odd $\tilde{N}_3$. If $\tilde{N}_3$ is even, topologically protected edge states occur, but they do not belong to the Majorana type. This is in agreement with the calculation of conditions for the formation of zeroth modes in the cylindrical topology.

The (chemical potential–exchange field) phase diagram with different topologically nontrivial phases is shown in Fig. 4. Each region located between two boundary lines is characterized by an individual value of the topological index $\tilde{N}_3$ indicated in the diagram. Solid lines are obtained from the condition of presence of gapless excitations in the toroidal topology. The parameters are the same as for Fig. 3. It is seen that an increase in the chemical potential results in a number of quantum topological transitions.

Analysis of zeros of the excitation spectrum in the phase of coexistence of superconductivity and noncollinear magnetic order significantly differs from analysis of the spectrum obtained in the Bardeen–Cooper–Schrieffer (BCS) theory. As mentioned in Section 2, the BCS spectrum has zero energy at edges and in the center of the hexagonal Brillouin zone only when the chemical potential crosses the bottom or top of the bare electron band. The spectrum in the phase of coexistence can have zeros at these points in view of the exchange field when the chemical potential lies inside the Brillouin zone. Such a situation is seen in Fig. 4 at the transition from the region with $\tilde{N}_3 = -2$ to the region with $\tilde{N}_3 = -3$ and at the $\tilde{N}_3 = 1 \to \tilde{N}_3 = 0$ transition when the gap is closed at the point $K_I$. This point corresponds to one of the nonequivalent points lying

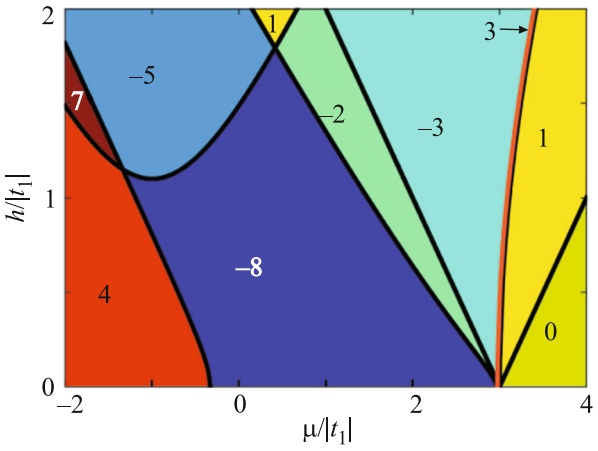


**Fig. 4.** (Color online) Diagrams of topological phases with the corresponding values of the $\tilde{N}_3$ invariant (see Eq. (13)).

on the intersection of the edges of the hexagonal Brillouin zone. In this case, $\Delta_d(\mathbf{k}) = \Delta_d(-\mathbf{k} + \mathbf{Q}) = 0$. The second such transition occurs between the regions with $N_3 = 3$ (this very narrow region is marked by the thick line between the regions with $\tilde{N}_3 = -3$ and $\tilde{N}_3 = 1$) and $\tilde{N}_3 = 1$ when the gap in the spectrum is closed at the (0, 0) point (center of the Brillouin zone) and $(2\pi/3, 2\pi/3)$ (the second nonequivalent point at the edge of the Brillouin zone). The crossing of nodal points of the superconducting order parameter by the Fermi contour for the superconductor without magnetic order results in the formation of gapless excitations. When noncollinear magnetism is taken into account, this condition is not satisfied because the spectrum depends also on $\Delta_d(-\mathbf{k} + \mathbf{Q})$. However, there are conditions when the energy spectrum vanishes at points where the parameters $\Delta_d(\mathbf{k})$ and $\Delta_d(-\mathbf{k} + \mathbf{Q})$ are nonzero. Such a situation corresponds to the other transitions in Fig. 4.

Strong electron correlations should be taken into account in real materials with the phase of coexistence of $d + id$ chiral superconductivity and spin ordering. In [52], we not only demonstrated the stability of Majorana modes with respect to electron interactions but also determined their structure in the ensemble of Hubbard fermions of strongly correlated systems. In that work, the conditions of occurrence of topologically nontrivial phases were found from the solution of self-consistency equations for the order parameters.

## 4. CALORIC ANOMALIES AND THE FERMION PARITY OF THE NANOWIRE IN THE SUPERCONDUCTING PHASE WITH NONTRIVIAL TOPOLOGY

In the preceding section, considering one of the systems with $D$ symmetry, it was shown that change in external conditions for the region of parameters where

the topologically nontrivial phase occurs induces oscillations of the energy of the Fermi excitation. This leads to a nonmonotonic dependence of the thermodynamic characteristics, which can be used to identify the topologically nontrivial phase.

Candidates for the experimental detection of the topologically nontrivial phase are quasi-one-dimensional superconductors [5–7, 29]. Actively studied superconducting nanowires with induced *s*-wave superconductivity in the external magnetic field are among such systems. They are popular because of the developed molecular beam epitaxy technology. InAs or InSb wires with strong spin–orbit coupling and large *g*-factors ($g_{\mathrm{InAs}} \sim 10$–$25$ [57] and $g_{\mathrm{InSb}} \sim 20$–$70$ [58]), as well as standard BCS superconductors such as Al whose thin (5–10 nm) layers are deposited on the surface of a nanowire [59], are usually studied.

The progress in the fabrication of such hybrid structures allowed ballistic transport experiments [29]. A peak of the differential conductivity at zero voltage in a wide range of magnetic fields was detected with the height equal to two conductivity quanta, i.e., $2G_0$. This was treated as the formation of topologically nontrivial phases with Majorana modes [29]. However, such a resonance can appear because of the inhomogeneities of the electrostatic potential and Andreev reflection on them [60]. Since the interpretation of such experiments is ambiguous, the development of alternative methods of experimental identification of topologically nontrivial phases in superconducting nanowires is relevant.

A promising approach to the experimental detection of topologically nontrivial phases can be based on the study of magnetocaloric anomalies [61, 62]. The physical foundation of the method is change in the fermion parity of the ground state of the system under the variation of the external parameter.

We consider the superconducting nanowire described by the Hamiltonian [63]

$$\mathcal{H}_W = -\frac{1}{2}\sum_{l\sigma}\left[ta^+_{l\sigma}a_{l+1,\sigma} + \alpha\eta_\sigma a^+_{l\sigma}a_{l+1,\bar{\sigma}} + \mathrm{H.c.}\right] + \sum_l\left[\sum_\sigma \xi_\sigma a^+_{l\sigma}a_{l\sigma} + \left(\Delta a_{l\uparrow}a_{l\downarrow} - h_x a^+_{l\uparrow}a_{l\downarrow} + \mathrm{H.c.}\right)\right]. \quad (16)$$

Here, $h_x = g\mu_B H_x$, where $g$ is the Landé $g$-factor, $\mu_B$ is the Bohr magneton, and $H_x$ is the $x$ component of the external magnetic field (in this section, $h_x = 0$); the terms in the first line describe the one-dimensional system of fermions with the hopping integral $t/2$ and the Rashba spin–orbit coupling parameter $\alpha/2$; the terms in the second line describe the proximity-induced superconducting pairing potential with the amplitude $\Delta = |\Delta|\exp(i\theta)$ (in this section, $\theta = 0$ is taken) and the energy of the fermion on one site $\xi_\sigma = \epsilon_0 - \mu + \eta_\sigma h_z$ measured from the chemical potential $\mu$, where $\eta_\uparrow = 1$, $\eta_\downarrow = -1$, and $h_z = g\mu_B H_z$.

The simple analysis shows that four types of the function of the ground state ($\hat{G} = \prod_{0<k<\pi}\hat{R}_k$) are possible for an even number of sites depending on the parameters of the superconducting nanowire:

$$|\Psi_I\rangle = \hat{R}_0\hat{R}_\pi\hat{G}|0\rangle; \quad |\Psi_{II}\rangle = \hat{R}_0 a^+_{\pi\downarrow}\hat{G}|0\rangle;$$
$$|\Psi_{III}\rangle = a^+_{0\downarrow}\hat{R}_\pi\hat{G}|0\rangle; \quad |\Psi_{IV}\rangle = a^+_{0\downarrow}a^+_{\pi\downarrow}\hat{G}|0\rangle. \quad (17)$$

Here, the quadratic forms

$$\hat{R}_k = A_k + B_k a^+_{-k\downarrow}a^+_{k\uparrow} + C_k a^+_{k\downarrow}a^+_{-k\uparrow} + D_k a^+_{-k\uparrow}a^+_{k\uparrow} + F_k a^+_{-k\downarrow}a^+_{k\downarrow} + G_k a^+_{-k\downarrow}a^+_{k\uparrow}a^+_{k\downarrow}a^+_{-k\uparrow}. \quad (18)$$
$$\hat{R}_0 = A_0 + B_0 a^+_{0\downarrow}a^+_{0\uparrow}; \quad \hat{R}_\pi = A_\pi + B_\pi a^+_{\pi\downarrow}a^+_{\pi\uparrow}$$

generate the superposition of states with an even number of fermions. Therefore, the negative fermion parity of the ground state is determined only by the character of the filling of states with $k = 0$ and $\pi$.

The functions $|\Psi_I\rangle$ and $|\Psi_{IV}\rangle$ are represented in the form of superpositions of states with even numbers of fermions. Correspondingly, the Majorana number is $\mathcal{M} = 1$. The functions $|\Psi_{II}\rangle$ and $|\Psi_{III}\rangle$ are superpositions of states with odd numbers of fermions and the Majorana number is $\mathcal{M} = -1$.

The requirement that the energy of the states $|\Psi_{II}\rangle$ and $|\Psi_{III}\rangle$ be lower than the energy of the states $|\Psi_I\rangle$ and $|\Psi_{IV}\rangle$ gives the inequalities

$$\sqrt{|\Delta|^2 + (\mu - |t|)^2} < |h| < \sqrt{|\Delta|^2 + (\mu + |t|)^2}, \quad (19)$$

which were previously obtained from the analysis of the Majorana number. Under these conditions, the parameters of the superconducting nanowire are such that the topologically nontrivial phase occurs (regions *II* and *III* in Fig. 5).

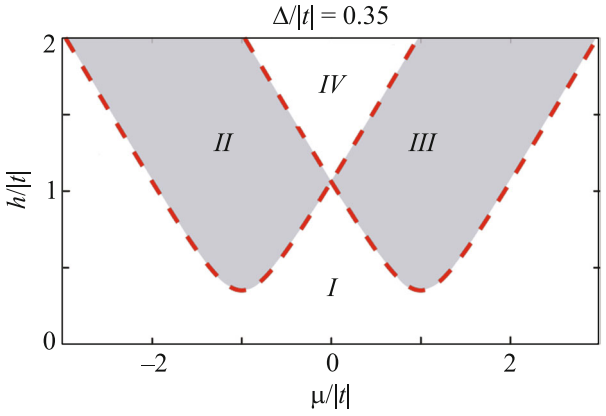


**Fig. 5.** (Color online) Diagrams of topological phases of the superconducting nanowire. Regions *II* and *III* correspond to topologically nontrivial phases ($\mathcal{M} = -1$), whereas regions *I* and *IV* correspond to a trivial topological phase ($\mathcal{M} = 1$).

Topologically protected Majorana modes with the exponentially low excitation energy $\varepsilon_0 \sim \exp(-N)$ occur in long open chains for the region of parameters corresponding to the topologically nontrivial phase in the closed geometry. The properties of these modes can be revealed by considering the expansion coefficients $w_{l\sigma,0}$ and $z_{l\sigma,0}$ of the self-adjoint operators $b' = \frac{1}{2}\left(\alpha_0 + \alpha_0^+\right)$ and $b'' = \frac{i}{2}\left(\alpha_0^+ - \alpha_0\right)$ in the single-site Majorana operators $\gamma_{Al\sigma}$ and $\gamma_{Bl\sigma}$:

$$\alpha_0 = \frac{1}{2}\sum_{l=1;\sigma}^{N}\left(w_{l\sigma,0}\gamma_{Al\sigma} + z_{l\sigma,0}\gamma_{Bl\sigma}\right);$$
$$w_{l\sigma,0} = e^{-i\theta/2}\left(u^*_{l\sigma,0} + v_{l\sigma,0}\right); \quad (20)$$
$$z_{l\sigma,0} = e^{-i\theta/2}\left(u^*_{l\sigma,0} - v_{l\sigma,0}\right),$$

where $u_{l\sigma,0}$ and $v_{l\sigma,0}$ are the Bogoliubov transformation coefficients. The overlapping of the distributions $w_{l\sigma,0}$ and $z_{l\sigma,0}$ is exponentially small. Correspondingly, Majorana modes are electrical- and spin-neutral because the electron and spin density distributions

$$\delta n_{l\sigma} = \langle 1|a^+_{l\sigma}a_{l\sigma}|1\rangle - \langle 0|a^+_{l\sigma}a_{l\sigma}|0\rangle = |u_{l\sigma,0}|^2 - |v_{l\sigma,0}|^2 = w_{l\sigma,0}z_{l\sigma,0}; \quad (21)$$

$$\delta s^z_l = \frac{1}{2}\sum_\sigma \eta_\sigma w_{l\sigma,0}z_{l\sigma,0}; \quad \delta s^x_l = \frac{1}{2}\sum_\sigma w_{l\sigma,0}z_{l\bar{\sigma},0}; \quad (22)$$

do not change at the transition of the superconducting nanowire from the ground state $|0\rangle$ to the state with the Majorana mode $|1\rangle = \alpha_0^+|0\rangle$.

The overlapping of the distributions $w_{l\sigma,0}$ and $z_{l\sigma,0}$ becomes significant as the length of the chain decreases. The energy of modes is generally nonzero, but excitations with zero energy are possible at certain parameters. As for the system specified by Eq. (9), these excitations occur on the lines bounding the shaded regions in Fig. 6. It is remarkable that the intersection of such lines is accompanied by change in the fermion parity of the ground state and a quantum transition occurs in the system. For this reason, the zeroth mode lines are lines of quantum critical points. The fermion parity $P$ is determined by the sign of the Pfaffian of the Bogoliubov–de Genes matrix $\tilde{H}$ of the Hamiltonian (16) written in the representation of Majorana operators:

$$P = \mathrm{sgn}\left(\mathrm{Pf}\left(\tilde{H}\right)\right). \quad (23)$$

The calculation of the fermion parity for the open nanowire provides the phase diagram shown in Fig. 6. The regions with $P = -1$ are shaded. Excitations with zero energy exist at the boundaries of these regions. All regions with $P = -1$ are located inside the region of the topologically nontrivial phase of the chain in the closed geometry. Consequently, the identification of lines of change in the fermion parity using the observable characteristics in the short open nanowire can indicate the region of the parameters where Majorana modes occur in the infinitely long open superconducting nanowire.

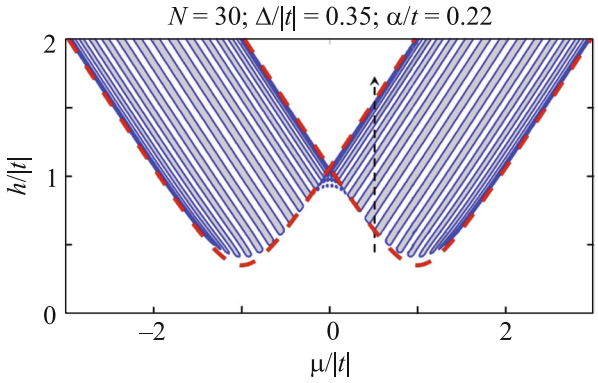


**Fig. 6.** (Color online) Phase diagram of the open superconducting nanowire. Regions with the negative fermion parity are shaded. The dashed lines are the boundaries of topologically nontrivial phases of the closed superconducting nanowire (see Fig. 5).

It is known that quantum transitions can be detected using the magnetocaloric effect [64, 65], which is manifested as change in the temperature of the system at the adiabatic variation of the magnetic field:

$$\left(\frac{\partial T}{\partial h}\right)_{S,\mu} = -T\left(\frac{\partial\langle M\rangle/\partial T}{C(T)}\right)_{\mu,h}, \quad (24)$$

where $\langle M\rangle$ is the specific magnetization and $C(T)$ is the specific heat. It is remarkable that the derivative (24) at low temperatures has different signs to the left and right of the quantum critical point and diverges at this point. Similar statements are valid for the electrocaloric effect, which is change in the temperature under the adiabatic variation of the electrochemical potential.

Correspondingly, caloric effects at low temperatures will demonstrate the described anomalous behavior when the external variable parameter is within the topologically nontrivial phase of the closed superconducting nanowire. This behavior is illustrated in Fig. 7, where the dashed lines are the dependences of caloric effects for the closed superconducting nanowire, where quantum transitions are accompanied by change in the topological index $\mathcal{M}$ and the solid lines are similar dependences for the open nanowire. These features can indicate the occurrence of the topologically nontrivial phase in the long superconducting nanowire and provide an additional criterion to the previously proposed tests (see, e.g., [29,

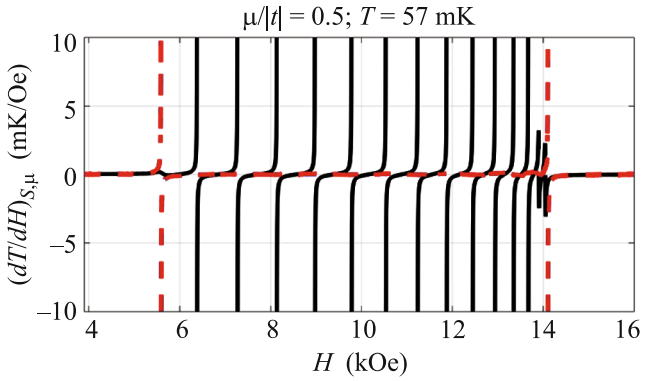


**Fig. 7.** (Color online) Field dependence of the magnetocaloric effect at the parameters $T = 10^{-3}|t|$, $\mu = 0.5|t|$, and other parameters same as in Fig. 6. Comparison with Fig. 6 indicates that the behavior of the caloric effect is anomalous in the region corresponding to the topologically nontrivial phase.

66]). The presented effects can occur not only in superconducting nanowires but also in other quasi-one-dimensional systems with $D$ symmetry.

## 5. FEATURES OF SPIN-POLARIZED TRANSPORT INVOLVING MAJORANA STATES

As mentioned above, the Majorana mode in long wires is characterized by zero average spin. At the same time, it was shown in some works that the transition to the topologically nontrivial phase can be identified either by observing separately the electron component of the spin polarization of the Majorana mode [67–69] or by studying the total spin polarization of all excitations except for the Majorana mode [70].

The nonzero electron (hole) spin polarization of the Majorana mode in transport processes is responsible for the equal-spin Andreev reflection [71– 73] and noncollinear Andreev reflection [74]. Thus, the existence of the Majorana mode can be tested by spin-polarized spectroscopy/microscopy.

In this context, we consider quantum transport in a ferromagnet/superconducting nanowire/ferromagnet system [75] described by the Hamiltonian

$$\mathcal{H} = \mathcal{H}_{\mathrm{L}} + \mathcal{H}_{\mathrm{R}} + \mathcal{H}_{\mathrm{W}} + \mathcal{H}_{\mathrm{T}}. \qquad (25)$$

Here, the first and second terms describe the left and right single-band ferromagnetic metal contacts in the Stoner model and have the form

$$\mathcal{H}_i = \sum_{k\sigma}\left[\xi_k - \frac{eV_i}{2} - \eta_\sigma M_i\right]c^+_{ik\sigma}c_{ik\sigma}, \quad i = \mathrm{L},\mathrm{R},$$

where $c^+_{ik\sigma}$ is the electron creation operator in the $i$th contact with the quasimomentum $k$, the spin projection on the quantization axis $\sigma$, and the energy $\xi_k = \epsilon_k - \mu$ ($\mu$ is the chemical potential of the system), and $M_i$ is the energy of the molecular field of the $i$th contact.

The term $\mathcal{H}_{\mathrm{W}}$ describes the superconducting nanowire with the Rashba spin–orbit coupling in a canted magnetic field ($h_x$, $h_z \neq 0$) and was introduced in Eq. (16). The term $\mathcal{H}_{\mathrm{T}}$ in Eq. (25) is the tunnel Hamiltonian describing the interaction between the superconducting wire and contacts and has the form

$$\mathcal{H}_{\mathrm{T}} = t_{\mathrm{L}}\sum_{k\sigma} c^+_{\mathrm{L}k\sigma}a_{1\sigma} + t_{\mathrm{R}}\sum_{p\sigma} c^+_{\mathrm{R}p\sigma}a_{N\sigma} + \mathrm{H.c.}, \qquad (26)$$

where $t_{\mathrm{L(R)}}$ is the tunnel coupling parameter between the left (right) contact and wire.

To analyze the transport properties, we use the nonequilibrium Green's function method [76–78]. For convenient description of the electron, hole, and spin degrees of freedom, we introduce four-component Nambu operators, $\psi_{im} = \left(d_{im\uparrow}d^+_{im\downarrow}d_{im\downarrow}d^+_{im\uparrow}\right)^T$, where $d_{im\sigma} = a_{j\sigma}, c_{ik\sigma}$ [74, 79]. Then, nonequilibrium Green's functions are represented in the form

$$G_{il,jm}(\tau,\tau') = -i\left\langle T_{\mathrm{C}}\psi_{il}(\tau)\otimes\psi^+_{jm}(\tau')\right\rangle, \qquad (27)$$

where $T_{\mathrm{C}}$ is the ordering operator on the Keldysh time contour. Using Eq. (27), the electron current in the $i$th contact is specified in the form

$$I_i = e\int_{-\infty}^{+\infty}\frac{d\omega}{\pi}\mathrm{Tr}\left[\mathrm{Re}\left\{\sigma\left(\Sigma^r_i G^<_{i,i} + \Sigma^<_i G^a_{i,i}\right)\right\}\right], \qquad (28)$$

where $\sigma = \mathrm{diag}(1,-1,1,-1)$ allows including contributions to the current from both the electron and hole channels; $\Sigma^{r(<)}_i = T^+_i g^{r(<)}_k T_i$ is the Fourier transform of the retarded self-energy function matrix (lesser functions), which describes the effect of the $i$th contact on the superconducting nanowire; and $g^{r(<)}_k$ is the Fourier transform of the retarded single-particle Green's function matrix (lesser functions) of the $i$th contact. Time-dependent tunnel coupling matrices have the form $T_i(t) = t_i\,\mathrm{diag}(e^{-ieV_it}, -e^{ieV_it}, e^{-ieV_it}, -e^{ieV_it})$. Further, $G^{a(<)}_{i,i} = P_i G^{a(<)}_W P^+_i$ is the $(i,i)$th block of the Fourier transform of the advanced Green's function matrix of the superconducting nanowire (lesser functions), which corresponds to its first (in the case of $I_{\mathrm{L}}$) or last (in the case of $I_{\mathrm{R}}$) site. These blocks are obtained using projection operators $P_{\mathrm{L}} = (IO)$ and $P_{\mathrm{R}} = (OI)$, where $I$ is the $4\times 4$ identity matrix and $O$ is the $4\times 4N-4$ zero block [80, 81].

The nonequilibrium Green's functions of the superconducting nanowire are determined by solving the Dyson and Keldysh equations

$$G^r = \left(\omega - H_W - \Sigma^r\right)^{-1}, \quad G^a = \left(G^r\right)^+, \tag{29}$$

$$G^{\lessgtr} = G^r\Sigma^{\lessgtr}G^a. \tag{30}$$

In Eq. (29), $H_W$ describes the superconducting nanowire in the space of Nambu operators. The total self-energy function of the system is written in the form $\Sigma^n = P_L^+\Sigma_L^n P_L + P_R^+\Sigma_R^n P_R$ $(n = r,a,>)$. Below, we consider semimetallic contacts (e.g., NiMnSb or $CrO_2$ [82]), which are characterized by the presence of charge carriers with only one spin projection (majority carriers). Then, the components referring to the $i$th contact in the wide-band approximation have the form $\Sigma_i^{r,a} = \mp\frac{i}{2}\Gamma_i = \text{const}$, $\Sigma_i^< = \left(\Sigma_i^a - \Sigma_i^r\right)F_i$, where $\Gamma_i = 2\pi t_i^2\rho_i$ is the parameter characterizing the broadening of the levels of the superconducting nanowire caused by coupling with the subband of majority carriers in the $i$th contact, $\rho_i$ is the density of states of the subband of majority carriers in the $i$th contact, and $F_i = \text{diag}\left(f_{i1}, f_{i2}, f_{i1}, f_{i2}\right)$, where $f_{i1,2}\left(\omega \pm eV_i/2\right)$ are the Fermi–Dirac functions.

In [75], we analyzed fluctuations of the current, in particular, shot noise at zero frequency [79, 83]:

$$\begin{aligned} S_i(0) = e^2\int_{-\infty}^{+\infty}\frac{d\omega}{\pi}\text{Tr}[&\sigma\Sigma_i^<\sigma G_{i,i}^> + G_{i,i}^<\sigma\Sigma_i^>\sigma \\ &- \sigma\left[\Sigma_i G_{i,i}\right]^<\sigma\left[\Sigma_i G_{i,i}\right]^> - \left[G_{i,i}\Sigma_i\right]^<\sigma\left[G_{i,i}\Sigma_i\right]^>\sigma \\ &+ \sigma\left[\Sigma_i G_{i,i}\Sigma_i\right]^>\sigma\hat{G}_{i,i}^< + G_{i,i}^>\sigma\left[\Sigma_i G_{i,i}\Sigma_i\right]^<\sigma]. \end{aligned} \tag{31}$$

We consider features of the conducting properties of the system under study. We assume that $V_L = V_R = V$. Then, certain transformations reduce Eq. (28) in the case of, e.g., the left contact to the form

$$\begin{aligned} I_L &= I_L^{LAR} + I_L^{CAR} \\ &= e\int_{-\infty}^{+\infty}\frac{d\omega}{2\pi}\left[\Gamma_L^2\left(\left|G_{1,4}^r\right|^2 + \left|G_{4,1}^r\right|^2\right)\right. \\ &\left. + \Gamma_L\Gamma_R\left(\left|G_{1,4N}^r\right|^2 + \left|G_{4,4N-3}^r\right|^2\right)\right](f_2 - f_1), \end{aligned} \tag{32}$$

where $f_{1,2} \equiv n\left(\omega \pm eV/2\right)$ and $G_{i,j}^r$ are the matrix elements of $G^r$.

The derived expression for the current includes two components: (i) the local current $I_L^{LAR} \sim \Gamma_L^2$ associated with the processes of local Andreev reflection (LAR) and (ii) the nonlocal current $I_L^{CAR} \sim \Gamma_L\Gamma_R$ associated with the processes of crossed Andreev reflection (CAR) [71, 74]. The matrix elements of the Fourier transform of the retarded Green's function, which are responsible for mentioned processes, have the form $G_{1,4}^r = \langle\langle a_{1\uparrow}|a_{1\uparrow}\rangle\rangle$ and $G_{1,4N}^r = \langle\langle a_{1\uparrow}|a_{N\uparrow}\rangle\rangle$. We emphasize that Andreev processes in the semimetal/superconductor system are absent except for the spin-flip processes because this type of ferromagnets has only one subband of charge carriers. However, e.g., if scattering on the interface allows spin-flip processes, Andreev reflection without change in the spin projection of carriers occurs [84, 85].

In the case of the superconducting nanowire under consideration, a nonzero contribution to the spin-polarized current from Andreev channels arises because of the spin–orbit coupling. We demonstrate this by considering the simplest situation where the superconducting nanowire consists of two sites ($N = 2$) and $h_x = 0$. Then, the numerators of the corresponding Green's functions have the form

$$\begin{aligned} \text{num}\left\{G_{1,4}^r\right\} &= -16\eta_\sigma\Delta\alpha t\xi_{\bar\sigma}\left[\omega\left(16\eta_\sigma\xi_0 h_z + \Gamma_R^2\right)\right. \\ &\left. + 2i\Gamma_R\left(\Delta^2 + \alpha^2 + t^2 - \omega^2 - \xi_{\bar\sigma}^2\right)\right], \\ \text{num}\left\{G_{1,4N}^r\right\} &= 32\eta_\sigma\Delta\alpha\xi_{\bar\sigma}\left[\left(\Delta^2 + \alpha^2 + t^2\right)^2\right. \\ &+ t^2\left(C_{e\bar\sigma}C_{h\bar\sigma} - \omega(4\omega + i\Gamma)\right) \\ &+ C_{e\sigma L}C_{h\sigma R}\left(t^2 + C_{e\bar\sigma}C_{h\bar\sigma}\right) \\ &- C_{e\sigma L}\left(\alpha^2 C_{e\bar\sigma} + \Delta^2 C_{h\bar\sigma}\right) \\ &\left. - C_{h\sigma R}\left(\alpha^2 C_{h\bar\sigma} + \Delta^2 C_{e\bar\sigma}\right)\right], \\ G_{4,1}^r &= G_{1,4}^r, \quad G_{4,4N-3}^r = -G_{1,4N}^r\left(L \longleftrightarrow R\right), \end{aligned} \tag{33}$$

where $C_{e\sigma L(h\sigma R)} = \omega \mp \xi_\sigma + i\Gamma_{L(R)}/2$, $C_{e(h)\bar\sigma} = \omega \mp \xi_{\bar\sigma}$, $\Gamma = \Gamma_L + \Gamma_R$, and $\xi_0 = t - \mu$. The lengthy denominator common for all Green's functions is not presented here. According to Eqs. (33), the local and crossed Andreev reflections from the semimetal/superconducting nanowire interface occur only if the superconducting nanowire demonstrates both superconducting pairing and spin–orbit coupling simultaneously.

In the single-contact geometry ($\Gamma_R = 0$), the current is determined only by local processes. For further consideration, it is important that the differential conductance $G_L = dI_L/dV$ in the linear response regime tends to zero. Such a behavior is in agreement with that described for the case where a superconductor (without the spin–orbit coupling) is in contact with a semimetal, where the magnetization gradient is perpendicular to the interface [84, 85]. At the same time, the contribution to the current from both channels in the nonlocal regime is nonzero at any $\omega$ values.

We further consider only the weakly nonequilibrium regime, $0 < eV/2 < \min(\delta\varepsilon_0)$, where $\delta\varepsilon_0$ stands for the maxima of the characteristic oscillatory depen-

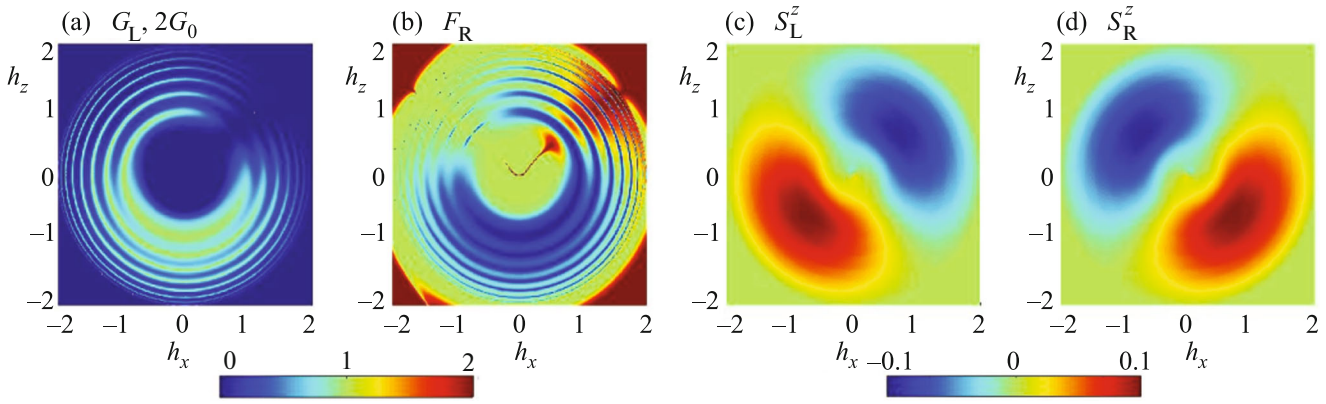


**Fig. 8.** (Color online) (a) Conductance of the left contact, (b) the Fano factor of the right contact, and (c, d) the $z$ component of the electron spin polarization of the Majorana mode on the (c) left, $S^z_L$, and (d) right, $S^z_R$, ends of the superconducting nanowire. Color scales are given under the respective panels. The parameters are $t = 1$, $\mu = 0$, $\Delta = 0.4$, $\alpha = 2$, and $N_0 = 30$.

dence of the excitation energy of Majorana modes on the external magnetic field. This dependence is due to the hybridization of distributions $w_{l\sigma,0}$ and $z_{l\sigma,0}$ introduced in Eqs. (20) and is manifested in magnetocaloric anomalies described above.

Figure 8a shows the dependence (conductance map) of the conductance of the left contact on the $x$ and $z$ components of the magnetic field perpendicular to the Rashba field vector. At a fixed orientation of the magnetic field **H**, an increase in the field strength is accompanied by an increase in $\delta\varepsilon_0$. In this case, the $2G_0$ maxima of the conductivity caused by local resonant Andreev reflection on Majorana modes ($G_L^{LAR} = 2G_0$, $G_L^{CAR} = 0$) [86] alternate with minima. The calculations for different directions of **H** show concentric resonance rings on the conductance map. The width of these rings depends on the direction of the field and all maxima of the conductance are suppressed for a certain orientation.

The calculations indicate that the transport of spin-polarized electrons (holes) with the energy near the Fermi level is determined by the behavior of the electron (hole) component of the spin polarization of Majorana modes at the ends of the superconducting nanowire, $(\delta s^z_{l(N)})_e \equiv S^z_{L(R)} = |u_{l(N)\uparrow,0}|^2 - |u_{l(N)\downarrow,0}|^2$ (for a fairly short wire with $N = 30$, $(\delta s^z_{l(N)})_e \approx -(\delta s^z_{l(N)})_h$). Figures 8c and 8d shows the magnetic field dependences of $S^z_L$ and $S^z_R$, respectively. In the lower half-plane, $S^z_{L,R} > 0$ because the field is antiparallel to the $z$ axis. As a result, conductance rings in this region are wider.

The comparison of Figs. 8a and 8c shows that resonances of $G_L(h_x, h_z)$ are suppressed at orientations of the magnetic fields for which $S^z_L$ has a minimum (see the dark blue region in Fig. 8c). It is important that $S^z_{L\uparrow} = |u_{l\uparrow,0}|^2 \approx 0$ in this case. As a result, the spin-polarized transport is suppressed and $I_L \approx 0$. At the same time, the polarization on the right end at the same field orientations tends to zero and $S^z_{R\uparrow} \approx -S^z_{R\downarrow} \neq 0$. The last property means that resonances in the conductance of the right contact $G_R$ that are caused by local Andreev reflection on Majorana modes hold, i.e., $I_R \neq 0$ (not shown in Fig. 8) [75].

Thus, for the indicated direction of the magnetic field, the transport regime is strongly asymmetric, close to single-contact, which is also confirmed by the behavior of the Fano factor of the right contact $F_R = S_R(0)/(2eI_R)$ shown in Fig. 8b. It is seen that, when $h_x \approx h_z$, magnetic fields at which $G_R \approx 2G_0$ correspond to $F_R = 0$. In the intervals between these minima, $F_R \to 2$. This indicates that local Andreev reflection dominates in regions with the low conductance [79, 86]. On the contrary, in all other regions, where the two-contact regime holds and $G_L$, $G_R \ll 1$, the processes of crossed Andreev reflection dominate and, as a result, $F_R \to 1$ [87].

We note that the breaking of the symmetry of currents observed at (also detected at the spin-independent transport via Majorana modes [88]) is characteristic just of the weakly nonequilibrium transport regime. Indeed, according to Eqs. (33), the linear response approximation in the single-contact regime gives $G_L = G_R = 0$ and $I_L = -I_R$.

A similar analysis can also be performed for the field orientation characterized by the relation $h_x \approx -h_z$ [75]. In this case, $I_L \neq 0$, $I_R \approx 0$. In other cases, $I_L = -I_R$. Thus, the performed analysis shows that the magnetic field allows controlling the direction of the spin-polarized current in a weakly nonequilibrium

semiconductor/superconducting nanowire/superconductor system if the device is in a topologically nontrivial phase.

## 6. CONCLUSIONS

The reported studies of the formation of topological phases in condensed matter have shown that the inclusion of the Coulomb interaction between electrons and noncollinear spin ordering gives new mechanisms of induction of states with nontrivial topology.

Conditions for the quantum topological transitions in $d + id$ chiral superconductors without magnetic order and in the phase of coexistence of $d + id$ superconductivity and noncollinear spin ordering have been analyzed. In the former case, topologically nontrivial phases have an even topological index. At parameters for which the state of the system is topologically nontrivial, edge states are formed in the case of open boundaries.

When the 120° magnetic order occurs, the regions of formation of topologically nontrivial phases change because phases with odd topological invariants appear. Edge states formed in open systems in such phases are Majorana states. The existence of a set of zeroth modes is important for experimental search for topologically nontrivial phases.

The study of the superconducting nanowire with the strong Rashba spin–orbit coupling and induced superconductivity has shown that the variation of the external magnetic field initiates an anomalous behavior of caloric effects in such a system only if the parameters of the nanowire correspond to a topologically nontrivial phase. The mentioned features are due to a cascade of quantum transitions with change in the fermion parity of the ground state of the system. This effect can be used as a new method of experimental identification of a topologically nontrivial phase in a nanowire.

Features of the transport characteristics of hybrid structures containing a superconducting nanowire in the topological phase have been analyzed. In particular, the semimetal/superconducting nanowire/semimetal structure exhibits the breaking of symmetry of currents caused by the formation of a topologically nontrivial phase. This phenomenon can be used to detect Majorana modes and to create a new generation of electronic devices.

## FUNDING

This work was supported by the Russian Foundation for Basic Research (project nos. 16-02-00073, 18-32-00443, 19-02-00348) and jointly by the Government of the Krasnoyarsk Territory, the Krasnoyarsk Regional Fund of Science (project no. 18-42-243017, "Manifestation of Coulomb Interactions and Effects of Bounded Geometry in the Properties of Topological Edge States of Nanostructures with Spin–Orbit Interaction"; project no. 18-42-243018, "Contact Phenomena and Magnetic Disorder in the Problem of the Formation and Detection of Topologically Protected Edge States in Semiconductor Nanostructures"; and project no. 18-42-240014, "Single-Orbit Effective Model of an Ensemble of Spin-Polaron Quasiparticles in the Problem of Describing the Intermediate State and Pseudogap Behavior of Cuprate Superconductors"). S.V. Aksenov and A.O. Zlotnikov acknowledge the support of the Council of the President of the Russian Federation for State Support of Young Scientists and Leading Scientific Schools (project nos. MK-3722.2018.2 and MK-3594.2018.2).

## REFERENCES

1. M. Z. Hasan and C. L. Kane, Rev. Mod. Phys. **82**, 3045 (2010).
2. Yu. E. Lozovik, Phys. Usp. **55**, 1035 (2012).
3. S. R. Elliott and M. Franz, Rev. Mod. Phys. **87**, 137 (2015).
4. N. Read and D. Green, Phys. Rev. B **61**, 10267 (2000).
5. A. Yu. Kitaev, Phys. Usp. **44**, 131 (2001).
6. J. D. Sau, R. M. Lutchyn, S. Tewari, and S. Das Sarma, Phys. Rev. Lett. **104**, 040502 (2010).
7. R. M. Lutchyn, J. D. Sau, and S. Das Sarma, Phys. Rev. Lett. **105**, 077001 (2010).
8. L. Fidkowski and A. Yu. Kitaev, Phys. Rev. B **81**, 134509 (2010).
9. S. Gangadharaiah, B. Braunecker, P. Simon, and D. Loss, Phys. Rev. Lett. **107**, 036801 (2011).
10. J. Klinovaja and D. Loss, Phys. Rev. B **90**, 045118 (2014).
11. T. Morimoto, A. Furusaki, and Ch. Mudry, Phys. Rev. B **92**, 125104 (2015).
12. M.-Y. Yao, L. Miao, N. L. Wang, J. H. Dil, M. Z. Hasan, D. D. Guan, C. L. Gao, C. Liu, D. Qian, and J. Jia, Phys. Rev. B **91**, 161411 (2015).
13. Y. Chen and H.-Y. Kee, Phys. Rev. B **97**, 085155 (2018).
14. Y. Sato, S. Matsuo, C.-H. Hsu, P. Stano, K. Ueda, Y. Takeshige, H. Kamata, J. S. Lee, B. Shojaei, K. Wickramasinghe, J. Shabani, C. Palmstrom, Y. Tokura, D. Loss, and S. Tarucha, Phys. Rev. B **99**, 155304 (2019).
15. J. Jang, D. G. Ferguson, V. Vakaryuk, R. Budakian, S. B. Chung, P. M. Goldbart, and Y. Maeno, Science (Washington, DC, U. S.) **331**, 186 (2011).
16. C. L. M. Wong and K. T. Law, Phys. Rev. B **86**, 184516 (2012).
17. I. Martin and A. F. Morpurgo, Phys. Rev. B **85**, 144505 (2012).
18. Y.-M. Lu and Z. Wang, Phys. Rev. Lett. **110**, 096403 (2013).
19. Y.-M. Lu, T. Xiang, and D.-H. Lee, Nat. Phys. **10**, 634 (2014).
20. A. Lau and C. Timm, Phys. Rev. B **90**, 024517 (2014).
21. Y. Nakajima, R. Hu, K. Kirshenbaum, A. Hughes, P. Syers, X. Wang, K. Wang, R. Wang, S. R. Saha, D. Pratt, J. W. Lynn, and J. Paglione, Sci. Adv. **1**, e1500242 (2015).

22. S. Sasaki and T. Mizushima, Phys. C (Amsterdam, Neth.) **514**, 206 (2015).
23. C. Youmans, A. Ghazaryan, M. Kargarian, and P. Ghaemi, Phys. Rev. B **98**, 144517 (2018).
24. S. Zhu, L. Kong, L. Cao, et al., arXiv:1904.06124 [cond-mat] (2019).
25. G. E. Volovik and V. M. Yakovenko, J. Phys.: Condens. Matter **1**, 5263 (1989).
26. C. Wang and T. Senthil, Phys. Rev. B **89**, 195124 (2014).
27. V. Mourik, K. Zuo, S. M. Frolov, S. R. Plissard, E. P. A. M. Bakkers, and L. P. Kouwenhoven, Science (Washington, DC, U. S.) **336**, 1003 (2012).
28. Y. Oreg, G. Refael, and F. von Oppen, Phys. Rev. Lett. **105**, 177002 (2010).
29. R. M. Lutchyn, E. P. A. M. Bakkers, L. P. Kouwenhoven, P. Krogstrup, C. M. Marcus, and Y. Oreg, Nat. Rev. Mater. **3**, 52 (2018).
30. K. Takada, H. Sakurai, E. Takayama-Muromachi, F. Izumi, R. A. Dilanian, and T. Sasaki, Nature (London, U.K.) **422**, 53 (2003).
31. N. B. Ivanova, S. G. Ovchinnikov, M. M. Korshunov, I. M. Eremin, and N. V. Kazak, Phys. Usp. **52**, 789 (2009).
32. V. V. Val'kov, T. A. Val'kova, D. M. Dzebisashvili, and S. G. Ovchinnikov, JETP Lett. **75**, 378 (2002).
33. R. O. Zaitsev, Sov. Phys. JETP **41**, 100 (1975).
34. R. O. Zaitsev, *Diagram Methods in Theory of Superconductivity and Ferromagnetism* (URSS, Moscow, 2004) [in Russian].
35. S. Zhou and Z. Wang, Phys. Rev. Lett. **100**, 217002 (2008).
36. W. Kohn and J. M. Luttinger, Phys. Rev. Lett. **15**, 524 (1965).
37. M. Yu. Kagan and A. V. Chubukov, JETP Lett. **47**, 614 (1988).
38. M. Yu. Kagan, V. A. Mitskan, and M. M. Korovushkin, Phys. Usp. **58**, 733 (2015).
39. P. W. Anderson, Phys. Rev. **110**, 827 (1958).
40. V. V. Val'kov, T. A. Val'kova, and V. A. Mitskan, JETP Lett. **102**, 361 (2015).
41. V. V. Val'kov, T. A. Val'kova, and V. A. Mitskan, J. Magn. Magn. Mater. **440**, 129 (2017).
42. G. E. Volovik, JETP Lett. **66**, 522 (1997).
43. B. Braunecker, G. I. Japaridze, J. Klinovaja, and D. Loss, Phys. Rev. B **82**, 045127 (2010).
44. T.-P. Choy, J. M. Edge, A. R. Akhmerov, and C. W. J. Beenakker, Phys. Rev. B **84**, 195442 (2011).
45. M. Kjaergaard, K. Wolms, and K. Flensberg, Phys. Rev. B **85**, 020503 (2012).
46. B. Braunecker and P. Simon, Phys. Rev. Lett. **111**, 147202 (2013).
47. J. Klinovaja, P. Stano, A. Yazdani, and D. Loss, Phys. Rev. Lett. **111**, 186805 (2013).
48. V. V. Val'kov and A. O. Zlotnikov, JETP Lett. **104**, 483 (2016).
49. K. Jiang, S. Zhou, and Z. Wang, Phys. Rev. B **90**, 165135 (2014).
50. K. Pasrija and S. Kumar, Phys. Rev. B **93**, 195110 (2016).
51. C. Weber, A. Lauchli, F. Mila, and T. Giamarchi, Phys. Rev. B **73**, 014519 (2006).
52. V. V. Val'kov and A. O. Zlotnikov, JETP Lett. **109**, 736 (2019).
53. V. V. Val'kov, A. O. Zlotnikov, and M. S. Shustin, J. Magn. Magn. Mater. **459**, 112 (2018).
54. A. P. Schnyder, S. Ryu, A. Furusaki, and A. W. W. Ludwig, Phys. Rev. B **78**, 195125 (2008).
55. K. Ishikawa and T. Matsuyama, Nucl. Phys. B **280**, 523 (1987).
56. P. Ghosh, J. D. Sau, S. Tewari, and S. Das Sarma, Phys. Rev. B **82**, 184525 (2010).
57. V. Aleshkin, V. Gavrilenko, A. Ikonnikov, S. Krishtopenko, Yu. G. Sadofyev, and K. E. Spirin, Semiconductors **42**, 828 (2008).
58. H. A. Nilsson, P. Caroff, C. Thelander, M. Larsson, J. B. Wagner, L.-E. Wernersson, L. Samuelson, and H. Q. Xu, Nano Lett. **9**, 3151 (2009).
59. M. T. Deng, S. Vaitiekenas, E. B. Hansen, J. Danon, M. Leijnse, K. Flensberg, J. Nygard, P. Krogstrup, and C. M. Marcus, Science (Washington, DC, U. S.) **354**, 1557 (2016).
60. C. Moore, C. Zeng, T. D. Stanescu, and S. Tewari, Phys. Rev. B **98**, 155314 (2018).
61. V. V. Val'kov, V. A. Mitskan, and M. S. Shustin, JETP Lett. **106**, 798 (2017).
62. V. V. Val'kov, V. A. Mitskan, and M. S. Shustin, Zh. Eksp. Teor. Fiz. **156**, 507 (2019).
63. E. M. Stoudenmire, J. Alicea, O. A. Starykh, and M. P. A. Fisher, Phys. Rev. B **84**, 014503 (2011).
64. L. Zhu, M. Garst, A. Rosch, and Q. Si, Phys. Rev. Lett. **91**, 066404 (2003).
65. M. Garst and A. Rosch, Phys. Rev. B **72**, 205129 (2005).
66. C. Beenakker, Ann. Rev. Condens. Matter Phys. **4**, 113 (2013).
67. D. Sticlet, C. Bena, and P. Simon, Phys. Rev. Lett. **108**, 096802 (2012).
68. M. Guigou, N. Sedlmayr, J. Aguiar-Hualde, and C. Bena, Eur. Phys. Lett. **115**, 47005 (2016).
69. E. Prada, R. Aguado, and P. San-Jose, Phys. Rev. B **96**, 085418 (2017).
70. M. Serina, D. Loss, and J. Klinovaja, Phys. Rev. B **98**, 035419 (2018).
71. A. F. Andreev, Sov. Phys. JETP **19**, 1228 (1964).
72. J. J. He, T. K. Ng, P. A. Lee, and K. T. Law, Phys. Rev. Lett. **112**, 037001 (2014).
73. J. J. He, J. Wu, T.-P. Choy, X.-J. Liu, Y. Tanaka, and K. T. Law, Nat. Commun. **5**, 3232 (2014).
74. B. H. Wu, W. Yi, J. C. Cao, and G.-C. Guo, Phys. Rev. B **90**, 205435 (2014).
75. V. V. Val'kov and S. V. Aksenov, J. Magn. Magn. Mater. **465**, 88 (2018).
76. L. V. Keldysh, Sov. Phys. JETP **20**, 1018 (1964).
77. S. Datta, *Electronic Transport in Mesoscopic Systems* (Cambridge Univ. Press, New York, 1995).
78. S. Datta, *Quantum Transport: Atom to Transistor* (Cambridge Univ. Press, New York, 2005).

79. B. H. Wu and J. C. Cao, Phys. Rev. B **85**, 085415 (2012).
80. V. V. Val'kov and S. V. Aksenov, Low Temp. Phys. **43**, 436 (2017).
81. V. V. Val'kov and S. V. Aksenov, J. Magn. Magn. Mater. **440**, 112 (2017).
82. R. S. Keizer, S. T. B. Goennenwein, T. M. Klapwijk, G. Miao, G. Xiao, and A. Gupta, Nature (London, U.K.) **439**, 825 (2006).
83. V. A. Khlus, Sov. Phys. JETP **66**, 1243 (1987).
84. B. Beri, J. N. Kupferschmidt, C. W. J. Beenakker, and P. W. Brouwer, Phys. Rev. B **79**, 024517 (2009).
85. J. N. Kupferschmidt and P. W. Brouwer, Phys. Rev. B **83**, 014512 (2011).
86. K. T. Law, P. A. Lee, and T. K. Ng, Phys. Rev. Lett. **103**, 237001 (2009).
87. J. Nilsson, A. R. Akhmerov, and C. W. J. Beenakker, Phys. Rev. Lett. **101**, 120403 (2008).
88. Y. Cao, P. Wang, G. Xiong, M. Gong, and X.-Q. Li, Phys. Rev. B **86**, 115311 (2012).

*Translated by R. Tyapaev*